A TOTAL VARIATION DISCONTINUOUS GALERKIN APPROACH FOR IMAGE RESTORATION

BENJAMIN STAMM AND THOMAS P. WIHLER

Abstract. The focal point of this paper is to propose and analyze a $\mathbb{P}_0$ discontinuous Galerkin (DG) formulation for image denoising. The scheme is based on a total variation approach which has been applied successfully in previous papers on image processing. The main idea of the new scheme is to model the restoration process in terms of a discrete energy minimization problem and to derive a corresponding DG variational formulation. Furthermore, we will prove that the method exhibits a unique solution and that a natural maximum principle holds. In addition, a number of examples illustrate the effectiveness of the method.

Key words. Discontinuous Galerkin methods, total variation image denoising, energy minimization methods, nonlinear elliptic filters.

1. Introduction

We consider a two dimensional display on which computer images can be visualized. Mathematically, this can be written in the form $\mathcal{S} = \{K\}$, where $\mathcal{S}$ corresponds to a screen, and $\{K\}$ is a set of disjoint open squares $\{K\}$ representing the pixels. A grayscale image on $\mathcal{S}$ is expressed in terms of a function

$$f : \mathcal{S} \to R,$$

where $R \subset \mathbb{R}$ is a compact interval that is determined by the range of all available grayscale values of the given visualization device.

Graphical data, as evaluated in medical applications, is typically bound to exhibit certain forms of defects which, when visualized on a computer screen, may manifest themselves, for example, in form of *noise* effects. A typical approach is to write

$$f = u + \eta,$$

where f is the perturbed image, u represents the denoised data, and η signifies some noise. A more general approach is given by $f = k * u + \eta$, where k is a convolution kernel that models certain types of blurring. In order to extract the relevant information (such as edges) behind image deficiencies, it is necessary to somehow restore the image f. More precisely, the improved image u is, on the one hand, supposed to contain the essential information of the original image f, and, on the other hand, should be cleaned from disturbing noise or blur.

The problem of image restoration has been tackled by means of several different techniques; let us refer the reader to the overview paper [3] for details. The approach that will be pursued in the present article is based on total variation image denoising. Such models have proved to be particularly effective in edge detection, see, e.g., [2, 5, 6, 9, 10, 11, 12, 13, 14]. Here, as remarked earlier, the basic idea is to take two (competing) aspects into account: First of all, the processed image u is supposed to be close to the original data f. This is accomplished, for instance, by controlling the difference between the two data sets with respect to a certain

distance measure $\|.\|_{\mathcal{S}}$ on $\mathcal{S}$, i.e., $\|u - f\|_{\mathcal{S}}$. Furthermore, it is desirable that the new image u is suitably denoised when compared to f. In variation based image denoising, supposing for a moment that u is sufficiently smooth on $\mathcal{S}$, this is usually modeled by appropriately bounding the gradient of u, e.g., in the form

$$\int_{\mathcal{S}} \phi(|\nabla u|)\, \mathrm{d}\boldsymbol{x}.$$

Here,

$$\phi: \mathbb{R}_{\geq 0} \to \mathbb{R}_{\geq 0}$$

is a given function that determines the smoothing process. Combining these two issues, an image restoration formulation is now obtained by minimizing the functional

$$\text{(1)} \qquad\qquad \mathsf{F}(u) = \|u - f\|_{\mathcal{S}} + \alpha \int_{\mathcal{S}} \phi(|\nabla u|)\, \mathrm{d}\boldsymbol{x},$$

where $\alpha \geq 0$ is a fixed constant, with respect to some appropriate function space. Subsequently, by applying standard variational calculus techniques, the above problem can be transformed into an Euler-Lagrange partial differential equation (PDE) formulation which, in turn, can be solved numerically.

In the present article, given the finite dimensional nature of computer images, we propose to formulate the minimization problem (1) directly on a discrete level, i.e., without employing the continuous PDE setting; see also, e.g., [4] for a related approach based on finite difference schemes. Here, we will introduce an energy functional on the discrete space $\mathbb{P}_0$ of all pixel-wise constant functions that features similar properties as the continuous functional F from (1). Then, a corresponding discrete variational formulation is derived. The novelty of our approach is to apply the framework of discontinuous Galerkin methods (see, e.g. [1] and the references therein), which constitute a natural choice in dealing with the discontinuous nature of pixel images, particularly in the context of edge detection. Moreover, the variational framework provides a quite handy setting for the analysis of the well-posedness of the proposed scheme and the derivation of a maximum principle.

The article is outlined as follows: In Section 2 the discrete model is presented. Furthermore, in Section 3 a discontinuous Galerkin formulation is derived and its well-posedness is established. In addition, a maximum principle for the method under consideration will be proved and a number of numerical examples illustrating our approach will be given in Section 4. Finally, we add a few concluding remarks in Section 5.

2. A Discrete Image Denoising Model

In the following section, we will establish a suitable mathematical setting, and the discrete image restoration model will be introduced.

2.1. Mathematical framework. Throughout the manuscript, we will suppose that the screen $\mathcal{S}$ consists of $m \times n$ (open and disjoint) pixels $K_{i,j} \subset \mathbb{R}^2$,

$$\mathcal{S} = \{K_{i,j}\}_{1 \leq i \leq m, 1 \leq j \leq n},$$

such that

$$\bigcup_{i,j} \overline{K}_{i,j}$$

is a closed rectangle. Each pixel is an open axiparallel square of length $h > 0$ that is given by

$$K_{i,j} = ((i-1)h, ih) \times ((j-1)h, jh), \qquad 1 \leq i \leq m,\, 1 \leq j \leq n.$$

The midpoint of $K_{i,j}$ is denoted by $\boldsymbol{x}_{i,j}$. It is reasonable to assume that the values of an image f are constant on each pixel, i.e., f belongs to the space

$$\mathbb{P}_0(\mathcal{S}) = \{v : \mathcal{S} \to \mathbb{R} : v|_K = \text{constant } \forall K \in \mathcal{S}\}$$

of all piecewise constant functions on $\mathcal{S}$. By $v_{i,j}$ we will signify the (grayscale) value of $v \in \mathbb{P}_0(\mathcal{S})$ on a pixel $K_{i,j}$, i.e., $v_{i,j} = v|_{K_{i,j}}$. Moreover, let us write $\boldsymbol{n}_{i,j}$ or $\boldsymbol{n}_{K_{i,j}}$ to denote the unit outward normal vector on $\partial K_{i,j}$, where $\partial K_{i,j}$ denotes the boundary of the pixel $K_{i,j}$. Furthermore, by $\mathcal{E}_{\text{int}}$ we define the set of all interior pixel edges in the screen:

$$\mathcal{E}_{\text{int}} = \{e : e = \partial K_{i,j} \cap \partial K_{i',j'}, \ K_{i,j}, K_{i',j'} \in \mathcal{S}\}.$$

Then, in order to compare the values of two neighboring pixels, we introduce the following (vector-valued) jump operator on $\mathcal{E}_{\text{int}}$: given an image $v \in \mathbb{P}_0(\mathcal{S})$, for an edge $e \in \mathcal{E}_{\text{int}}$ that is shared by two pixels $K_{i,j}$ and $K_{i',j'}$, we let

$$[\![v]\!]|_e = v_{i,j}\boldsymbol{n}_{i,j} + v_{i',j'}\boldsymbol{n}_{i',j'}.$$

We remark that this notation is very popular within the context of discontinuous Galerkin approaches; see, e.g., [1].

Furthermore, $\|.\|_{\mathcal{S}}$ is an L^2-type norm on $\mathbb{P}_0(\mathcal{S})$ given by

$$\|v\|_{\mathcal{S}}^2 = (v,v)_{\mathcal{S}}, \qquad v \in \mathbb{P}_0(\mathcal{S}),$$

where, for $v, w \in \mathbb{P}_0(\mathcal{S})$,

$$(v,w)_{\mathcal{S}} = \int_{\mathcal{S}} vw \, \mathrm{d}\boldsymbol{x} = h^2 \sum_{i,j} v_{i,j}w_{i,j}$$

is the L^2 product.

2.2. Discrete Functional. In order to obtain the image restoration model in this paper, we begin with introducing a discrete version of the gradient operator appearing in the continuous functional (1). In consequence, it is possible to define a corresponding discrete functional. For simplicity, in this paper, we restrict ourselves to noisy images without blur; we note however, that the proposed numerical scheme can be extended straightforwardly to a more general situation by including a discrete convolution kernel.

2.2.1. Discrete Gradients. The key point in image denoising is to suitably incorporate the smoothness of the restored image. Evidently, within the discrete space $\mathbb{P}_0(\mathcal{S})$ of piecewise constant functions, the gradient occurring in the functional F from (1) makes little sense. Taking the viewpoint of difference quotients, however, the jump of an image $v \in \mathbb{P}_0(\mathcal{S})$ along an edge $e \in \mathcal{E}_{\text{int}}$ is related to a discrete derivative. We make use of this observation to propose the following discrete gradient:

$$\nabla_{\mathcal{S}} v|_e := h^{-1}[\![v]\!]|_e,$$

for any $e \in \mathcal{E}_{\text{int}}, v \in \mathbb{P}_0(\mathcal{S})$.

Similarly, like in the functional F from (1), the smoothness of the image u to be restored is controlled by means of a function $\phi : \mathbb{R}_{\geq 0} \to \mathbb{R}_{\geq 0}$ in the form

$$v \mapsto \int_{\mathcal{E}_{\text{int}}} \phi\big(\big|h^{-1}[\![v]\!]|_e\big|\big) \, \mathrm{d}s,$$

where $\int_{\mathcal{E}_{\text{int}}}$ is understood as $\sum_{e \in \mathcal{E}_{\text{int}}} \int_e$.

Throughout the paper, the following assumptions on ϕ are imposed:

(a) $\phi \in C^1([0,\infty))$;

(b) ϕ and ϕ' are both nondecreasing;

(c) there exists a constant $L_\phi \geq 0$ such that

$$
(2) \qquad \left| \frac{\phi'(s) - \phi'(t)}{s - t} \right| \leq L_\phi,
$$

for any $s > t \geq 0$;

(d) the function

$$
(3) \qquad \psi : \mathbb{R}_{\geq 0} \to \mathbb{R}_{\geq 0}, \qquad \psi(x) = \begin{cases} \frac{\phi'(x)}{x}, & x > 0 \\ \lim_{t \to 0^+} \frac{\phi'(t)}{t}, & x = 0 \end{cases}
$$

is continuous on $[0, \infty)$. In particular, $\phi'(0) = 0$. Furthermore, by the monotonicity of ϕ' it follows that

$$
(4) \qquad (s\psi(s) - t\psi(t))(s - t) \geq 0,
$$

for any $s, t \geq 0$.

To give some examples of functions ϕ that are applicable in total variation image restoration and for which the above conditions are satisfied, we mention the approach by Rudin and Osher [11],

$$
(5) \qquad \phi_{\mathrm{RO}}(s) = \sqrt{s^2 + \beta},
$$

where $\beta > 0$ is a constant. Moreover, let us define

$$
(6) \qquad \phi_{\mathrm{CL}}(s) = \begin{cases} -\frac{s^3}{3\varepsilon^2} + \frac{s^2}{\varepsilon} + \frac{\varepsilon}{3}, & s \leq \varepsilon \\ s, & s > \varepsilon, \end{cases}
$$

for a parameter $\varepsilon > 0$; this is very closely related to an idea proposed by Chambolle and Lions [5].

2.2.2. Minimization Problem. We propose the following discrete analog of the functional F from (1):

$$
(7) \quad \mathsf{F}_{\mathrm{DG}} : \mathbb{P}_0(\mathcal{S}) \to \mathbb{R}_{\geq 0}, \qquad \mathsf{F}_{\mathrm{DG}}(v) = \frac{1}{2} \|v - f\|_{\mathcal{S}}^2 + \frac{\alpha h}{2} \int_{\mathcal{E}_{\mathrm{int}}} \phi(|h^{-1} [\![v]\!]|) \, \mathrm{d}s.
$$

For a given smoothing function ϕ, the intensity of the smoothing is controlled by means of the constant $\alpha \geq 0$. Then, our image restoration model reads: Given a noisy image $f \in \mathbb{P}_0(\mathcal{S})$, a denoised image $u \in \mathbb{P}_0(\mathcal{S})$ is obtained by solving the problem

$$
(8) \qquad u \in \mathbb{P}_0(\mathcal{S}) : \qquad \mathsf{F}_{\mathrm{DG}}(u) = \min_{v \in \mathbb{P}_0(\mathcal{S})} \mathsf{F}_{\mathrm{DG}}(v).
$$

Evidently, due to the finite dimension of $\mathbb{P}_0(\mathcal{S})$, this problem is discrete. The well-posedness of this formulation (which depends on the smoothing function ϕ) will be discussed in Section 3.2.

3. Discontinuous Galerkin Variational Formulation

In this section we will derive and analyze the variational form of (8).

3.1. Discontinuous Galerkin Method. Supposing that a minimizer $u \in \mathbb{P}_0(\mathcal{S})$ of F_{DG} exists, there holds

$$\left.\frac{\mathrm{d}}{\mathrm{d}\varepsilon}\mathsf{F}_{\mathrm{DG}}(u + \varepsilon w)\right|_{\varepsilon=0} = 0$$

for any $w \in \mathbb{P}_0(\mathcal{S})$. Computing the derivative of F_{DG} with respect to the scalar parameter ε, this immediately implies that u satisfies the variational formulation

$$(9) \qquad a_{\mathrm{DG}}(u, w) = (f, w)_{\mathcal{S}} \qquad \forall w \in \mathbb{P}_0(\mathcal{S}),$$

where

$$(10) \qquad a_{\mathrm{DG}}(u, w) = (u, w)_{\mathcal{S}} + \frac{\alpha}{2h}\int_{\mathcal{E}_{\mathrm{int}}} \psi(h^{-1}|[\![u]\!]|)[\![u]\!] \cdot [\![w]\!]\,\mathrm{d}s$$

is a (nonlinear) discontinuous Galerkin form. Notice that the choice $\alpha = 0$ leads the noisy image to be left unchanged.

In the sequel, we will deal with the image denoising model (8) by solving the discontinuous Galerkin formulation (9).

3.2. Existence and Uniqueness of Solutions. In order to show the well-posedness of the discontinuous Galerkin formulation (9), we will prove that the form a_{DG} is continuous and coercive. To this end, we start by deriving two technical lemmas.

Lemma 3.1. *Let $n \in \mathbb{N}$. The function ψ from* (3) *satisfies the bounds*

$$(11) \qquad |\psi(|\boldsymbol{x}|)\boldsymbol{x} - \psi(|\boldsymbol{y}|)\boldsymbol{y}| \leq L_\phi\,|\boldsymbol{x} - \boldsymbol{y}|\,,$$

and

$$(12) \qquad (\psi(|\boldsymbol{x}|)\boldsymbol{x} - \psi(|\boldsymbol{y}|)\boldsymbol{y}) \cdot (\boldsymbol{x} - \boldsymbol{y}) \geq 0,$$

for any $\boldsymbol{x}, \boldsymbol{y} \in \mathbb{R}^n$. Here, L_ϕ is the constant from (2).

Proof. The proof follows along the lines of [7, Lemma 2.1] and will be presented for completeness. In the scalar case, $n = 1$, the above estimates simply result from (2) and from (4).

Let now $n \geq 1$, and $|\boldsymbol{x}| \geq |\boldsymbol{y}| \geq 0$. Then, there holds

$$|\psi(|\boldsymbol{x}|)\boldsymbol{x} - \psi(|\boldsymbol{y}|)\boldsymbol{y}|^2 = (\psi(|\boldsymbol{x}|)|\boldsymbol{x}| - \psi(|\boldsymbol{y}|)|\boldsymbol{y}|)^2 + 2\psi(|\boldsymbol{x}|)\psi(|\boldsymbol{y}|)(|\boldsymbol{x}||\boldsymbol{y}| - \boldsymbol{x} \cdot \boldsymbol{y}).$$

Recalling the scalar case, we obtain

$$\begin{aligned}
(\psi(|\boldsymbol{x}|)|\boldsymbol{x}| - \psi(|\boldsymbol{y}|)|\boldsymbol{y}|)^2 &\leq L_\phi^2\,\big||\boldsymbol{x}| - |\boldsymbol{y}|\big|^2 \\
&= L_\phi^2\left(|\boldsymbol{x}|^2 - 2\boldsymbol{x} \cdot \boldsymbol{y} + |\boldsymbol{y}|^2\right) + 2L_\phi^2(\boldsymbol{x} \cdot \boldsymbol{y} - |\boldsymbol{x}||\boldsymbol{y}|) \\
&= L_\phi^2|\boldsymbol{x} - \boldsymbol{y}|^2 + 2L_\phi^2(\boldsymbol{x} \cdot \boldsymbol{y} - |\boldsymbol{x}||\boldsymbol{y}|).
\end{aligned}$$

Furthermore, we have that

$$0 \leq \psi(|\boldsymbol{x}|) \leq |\boldsymbol{x}|^{-1}\left(\psi(|\boldsymbol{x}|)|\boldsymbol{x}| - \psi(|\boldsymbol{0}|)|\boldsymbol{0}|\right) \leq L_\phi,$$

and, by the Cauchy-Schwarz inequality, that $|\boldsymbol{x}||\boldsymbol{y}| - \boldsymbol{x} \cdot \boldsymbol{y} \geq 0$. Consequently, combining these bounds yields

$$\begin{aligned}
|\psi(|\boldsymbol{x}|)\boldsymbol{x} - \psi(|\boldsymbol{y}|)\boldsymbol{y}|^2 &\leq L_\phi^2|\boldsymbol{x} - \boldsymbol{y}|^2 + 2(\psi(|\boldsymbol{x}|)\psi(|\boldsymbol{y}|) - L_\phi^2)(|\boldsymbol{x}||\boldsymbol{y}| - \boldsymbol{x} \cdot \boldsymbol{y}) \\
&\leq L_\phi^2|\boldsymbol{x} - \boldsymbol{y}|^2.
\end{aligned}$$

This corresponds to (11).

Moreover, in order to prove (12), we notice that

$$\begin{aligned}
(\psi(|\boldsymbol{x}|)\boldsymbol{x} - \psi(|\boldsymbol{y}|)\boldsymbol{y}) \cdot (\boldsymbol{x} - \boldsymbol{y}) &= (\psi(|\boldsymbol{x}|)|\boldsymbol{x}| - \psi(|\boldsymbol{y}|)|\boldsymbol{y}|)\,(|\boldsymbol{x}| - |\boldsymbol{y}|) \\
&\quad + (\psi(|\boldsymbol{x}|) + \psi(|\boldsymbol{y}|))\,(|\boldsymbol{x}||\boldsymbol{y}| - \boldsymbol{x} \cdot \boldsymbol{y}).
\end{aligned}$$

Applying once again the scalar inequality leads to

$$(\psi(|\boldsymbol{x}|)|\boldsymbol{x}| - \psi(|\boldsymbol{y}|)|\boldsymbol{y}|)\,(|\boldsymbol{x}| - |\boldsymbol{y}|) \geq 0.$$

Finally, using the Cauchy-Schwarz inequality as before, completes the proof of the lemma. □

The second lemma is a trace estimate on $\mathbb{P}_0(\mathcal{S})$.

Lemma 3.2. *There holds*

$$\int_{\mathcal{E}_{\mathrm{int}}} |[\![v]\!]|^2 \, \mathrm{d}s \leq 8h^{-1} \, \|v\|_{\mathcal{S}}^2$$

for any $v \in \mathbb{P}_0(\mathcal{S})$.

Proof. Applying the inequality $(a+b)^2 \leq 2(a^2+b^2)$, for any $a,b \in \mathbb{R}$, to the jump terms on the left-hand side of the desired bound, we have that

$$h \int_{\mathcal{E}_{\mathrm{int}}} |[\![v]\!]|^2 \, \mathrm{d}s = h^2 \sum_{e \in \mathcal{E}_{\mathrm{int}}} |[\![v]\!]|_e|^2 \leq 8h^2 \sum_{i,j} v_{i,j}^2 = 8\,\|v\|_{\mathcal{S}}^2\,.$$

This shows the asserted trace inequality. □

We are now ready to turn to the continuity and coercivity of the form a_{DG}.

Proposition 3.3. *The form a_{DG} is continuous and coercive in the sense that*

$$|a_{\mathrm{DG}}(u,w) - a_{\mathrm{DG}}(v,w)| \leq \left(1 + \frac{4\alpha L_\phi}{h^2}\right) \|u-v\|_{\mathcal{S}} \, \|w\|_{\mathcal{S}}\,,$$

and

$$(13) \qquad a_{\mathrm{DG}}(u, u-v) - a_{\mathrm{DG}}(v, u-v) \geq \|u-v\|_{\mathcal{S}}^2\,,$$

respectively, for any $u,v,w \in \mathbb{P}_0(\mathcal{S})$. Here, α and L_ϕ are the constants from (7) and (2), respectively.

Proof. We begin with showing the first bound. There holds

$$|a_{\mathrm{DG}}(u,w) - a_{\mathrm{DG}}(v,w)|$$
$$\leq |(u-v,w)_{\mathcal{S}}| + \left|\frac{\alpha}{2h}\int_{\mathcal{E}_{\mathrm{int}}} \left(\psi(h^{-1}|[\![u]\!]|)[\![u]\!] - \psi(h^{-1}|[\![v]\!]|)[\![v]\!]\right)\cdot[\![w]\!]\,\mathrm{d}s\right|$$
$$\leq \|u-v\|_{\mathcal{S}}\,\|w\|_{\mathcal{S}} + \frac{\alpha}{2h}\int_{\mathcal{E}_{\mathrm{int}}} \left|\psi(h^{-1}|[\![u]\!]|)[\![u]\!] - \psi(h^{-1}|[\![v]\!]|)[\![v]\!]\right||[\![w]\!]|\,\mathrm{d}s.$$

Applying (11) as well as the Cauchy-Schwarz inequality, we obtain

$$|a_{\mathrm{DG}}(u,w) - a_{\mathrm{DG}}(v,w)|$$
$$\leq \|u-v\|_{\mathcal{S}}\,\|w\|_{\mathcal{S}} + \frac{\alpha}{2}\int_{\mathcal{E}_{\mathrm{int}}} \left|\psi(h^{-1}|[\![u]\!]|)h^{-1}[\![u]\!] - \psi(h^{-1}|[\![v]\!]|)h^{-1}[\![v]\!]\right||[\![w]\!]|\,\mathrm{d}s$$
$$\leq \|u-v\|_{\mathcal{S}}\,\|w\|_{\mathcal{S}} + \frac{\alpha L_\phi}{2h}\int_{\mathcal{E}_{\mathrm{int}}} |[\![u-v]\!]||[\![w]\!]|\,\mathrm{d}s$$
$$\leq \left(\|u-v\|_{\mathcal{S}}^2 + \frac{\alpha L_\phi}{2h}\int_{\mathcal{E}_{\mathrm{int}}} |[\![u-v]\!]|^2\,\mathrm{d}s\right)^{\frac{1}{2}}\left(\|w\|_{\mathcal{S}}^2 + \frac{\alpha L_\phi}{2h}\int_{\mathcal{E}_{\mathrm{int}}} |[\![w]\!]|^2\,\mathrm{d}s\right)^{\frac{1}{2}}.$$

Then, applying Lemma 3.2, leads to

$$|a_{\mathrm{DG}}(u,w) - a_{\mathrm{DG}}(v,w)| \leq \left(1 + \frac{4\alpha L_\phi}{h^2}\right) \|u-v\|_{\mathcal{S}} \, \|w\|_{\mathcal{S}}\,.$$

This is the first bound. In order to derive the second estimate, we employ (12) to derive

$$a_{\mathrm{DG}}(u, u - v) - a_{\mathrm{DG}}(v, u - v)$$

$$= \|u - v\|_{\mathcal{S}}^2$$

$$+ \frac{\alpha h}{2} \int_{\mathcal{E}_{\mathrm{int}}} \left(\psi(h^{-1}|\llbracket u \rrbracket|) h^{-1} \llbracket u \rrbracket - \psi(h^{-1}|\llbracket v \rrbracket|) h^{-1} \llbracket v \rrbracket \right) \cdot \left(\llbracket h^{-1} u \rrbracket - \llbracket h^{-1} v \rrbracket \right) \, \mathrm{d}s$$

$$\geq \|u - v\|_{\mathcal{S}}^2 \,,$$

which completes the proof. $\qquad\square$

Applying [15, Theorem 2.H], for example, in combination with the above Proposition 3.3, implies the well-posedness of the discontinuous Galerkin formulation (9).

Theorem 3.4. *Under the previous assumptions on the function ψ, there exists a unique solution of the total variation discontinuous Galerkin method* (9) *in $\mathbb{P}_0(\mathcal{S})$.*

Remark 3.5. Referring to [8, Proof of Theorem 3.3.23], the fixed point iteration

$$(u_{n+1}, w)_{\mathcal{S}} = (u_n, w)_{\mathcal{S}} + \varepsilon \left((u_n - f, w)_{\mathcal{S}} + \frac{\alpha}{2h} \int_{\mathcal{E}_{\mathrm{int}}} \psi \left(h^{-1} |\llbracket u_n \rrbracket| \right) \llbracket u_n \rrbracket \cdot \llbracket w \rrbracket \, \mathrm{d}s \right)$$

for all $w \in \mathbb{P}_0(\mathcal{S})$, converges to the solution of (9) for any starting image $u_0 \in \mathbb{P}_0(\mathcal{S})$ and any $0 < \varepsilon < 2 \left(1 + \frac{4\alpha L_\phi}{h^2} \right)^{-2}$. We note, however, that the minimal reduction factor for the error in each step, which is given by

$$\varrho = \sqrt{1 - \left(1 + \frac{4\alpha L_\phi}{h^2} \right)^{-2}},$$

is typically very close to 1, and the iteration will converge at a very slow pace. In consequence, in our numerical experiments, an alternative fixed point iteration will be applied; see Section 4.

3.3. A Maximum Principle. The following result states that the color range of the denoised image u from (9) will be within the grayscale range of the original image f.

Theorem 3.6. *Let $f \in \mathbb{P}_0(\mathcal{S})$ be a (noisy) image and u its denoised version obtained from* (9). *Then, the inequality*

$$\inf_{\mathcal{S}} f \leq u \leq \sup_{\mathcal{S}} f$$

holds true on $\mathcal{S}$.

Proof. We prove the first bound only. The proof of the second one is similar. Let us suppose that there is a non-empty set $\mathcal{V}$ of pixels in $\mathcal{S}$ for which the first bound is violated:

$$\mathcal{V} = \{ K \in \mathcal{S} : \hat{v}|_K > 0 \}, \qquad \hat{v} := \max\{ \inf_{\mathcal{S}} f - u, 0 \}.$$

Clearly, we have that

$$0 < \int_{\mathcal{V}} (f - u) \hat{v} \, \mathrm{d}\boldsymbol{x} = \int_{\mathcal{S}} (f - u) \hat{v} \, \mathrm{d}\boldsymbol{x}.$$

Thence, invoking (9), it follows that

$$(14) \qquad 0 < \int_{\mathcal{E}_{\mathrm{int}}} \psi(h^{-1}|\llbracket u \rrbracket|) \llbracket u \rrbracket \cdot \llbracket \hat{v} \rrbracket \, \mathrm{d}s.$$

Let now $K \in \mathcal{S}$ be a pixel and $e \in \mathcal{E}_{\mathrm{int}}$ an interior edge of K. Furthermore, let $K' \in \mathcal{S}$ be the neighboring pixel of K which shares the edge e with K. In order to proceed, we distinguish three different cases.

(i) Suppose first that $K, K' \notin \mathcal{V}$. Then $\hat{v}|_{K \cup K'} = 0$ and thus, $[\![\hat{v}]\!]|_e = 0$. Hence,

$$\int_e \psi(h^{-1}|[\![u]\!]|)[\![u]\!] \cdot [\![\hat{v}]\!] \, \mathrm{d}s = 0.$$

(ii) If $K, K' \in \mathcal{V}$, then $[\![\hat{v}]\!]|_e = [\![\inf_{\mathcal{S}} f - u]\!]|_e = -[\![u]\!]|_e$. Thus, since ψ is nonnegative, we arrive at

$$\int_e \psi(h^{-1}|[\![u]\!]|)[\![u]\!] \cdot [\![\hat{v}]\!] \, \mathrm{d}s = -\int_e \psi(h^{-1}|[\![u]\!]|) \, |[\![u]\!]|^2 \, \mathrm{d}s \le 0.$$

(iii) Lastly, let us suppose that $K \in \mathcal{V}$ and $K' \notin \mathcal{V}$. In this case, we have that

$$[\![\hat{v}]\!] = \hat{v}|_K \boldsymbol{n}_K = (\inf_{\mathcal{S}} f - u)|_K \boldsymbol{n}_K.$$

Therefore,

$$[\![u]\!] \cdot [\![\hat{v}]\!] = (\inf_{\mathcal{S}} f - u)|_K \boldsymbol{n}_K \cdot (u|_K \boldsymbol{n}_K + u|_{K'} \boldsymbol{n}_{K'})$$

$$= (\inf_{\mathcal{S}} f - u)|_K \, (u|_K - u|_{K'})$$

$$= (\inf_{\mathcal{S}} f - u)|_K \left((u|_K - \inf_{\mathcal{S}} f) + (\inf_{\mathcal{S}} f - u|_{K'}) \right).$$

Furthermore, with

$$u|_K - \inf_{\mathcal{S}} f < 0, \qquad \inf_{\mathcal{S}} f - u|_{K'} \le 0,$$

we find that $[\![u]\!] \cdot [\![\hat{v}]\!] < 0$.

Consequently,

$$\int_{\mathcal{E}_{\mathrm{int}}} \psi(h^{-1}|[\![u]\!]|)[\![u]\!] \cdot [\![\hat{v}]\!] \, \mathrm{d}s \le 0.$$

which constitutes a contradiction to (14). $\square$

4. Numerical Examples

In the sequel, we will briefly discuss some implementational aspects of the proposed DG scheme. In addition, a few numerical results will be added.

4.1. Numerical Scheme. In order to solve the nonlinear system resulting from the DG formulation (9), we propose the following iteration scheme:

$$(15) \quad (u_{n+1} - f, w)_{\mathcal{S}} + \frac{\alpha}{2h} \int_{\mathcal{E}_{\mathrm{int}}} \psi\left(h^{-1}|[\![u_n]\!]|\right) [\![u_{n+1}]\!] \cdot [\![w]\!] \, \mathrm{d}s = 0 \qquad \forall w \in \mathbb{P}_0(\mathcal{S}).$$

The initial guess is chosen to be the noisy image, i.e., $u_0 = f$. This is a linear system for $u_{n+1} \in \mathbb{P}_0(\mathcal{S})$. Choosing basis functions

$$\xi_{i,j}(\boldsymbol{x}) = \begin{cases} h^{-2}, & \boldsymbol{x} \in K_{i,j} \\ 0, & \text{otherwise} \end{cases}, \qquad 1 \le i \le m, 1 \le j \le n,$$

for $\mathbb{P}_0(\mathcal{S})$, the $\mathcal{S}$-product in the above equation corresponds to an identity mass matrix $\boldsymbol{I}$, i.e.,

$$(\xi_{i,j}, \xi_{k,l})_{\mathcal{S}} = \delta_{(i,j),(k,l)},$$

where δ denotes Kronecker's delta. Furthermore, the bilinear form

$$(v, w) \mapsto \int_{\mathcal{E}_{\mathrm{int}}} \psi\left(h^{-1}|[\![u_n]\!]|\right) [\![v]\!] \cdot [\![w]\!] \, \mathrm{d}s$$

(a) Using ϕ_{RO} with $\beta = 0.1$.   (b) Using ϕ_{RO} with $\beta = $ 1e-4.

(c) Using ϕ_{CL} with $\varepsilon = 0.1$.   (d) Using ϕ_{CL} with $\varepsilon = $ 1e-4.
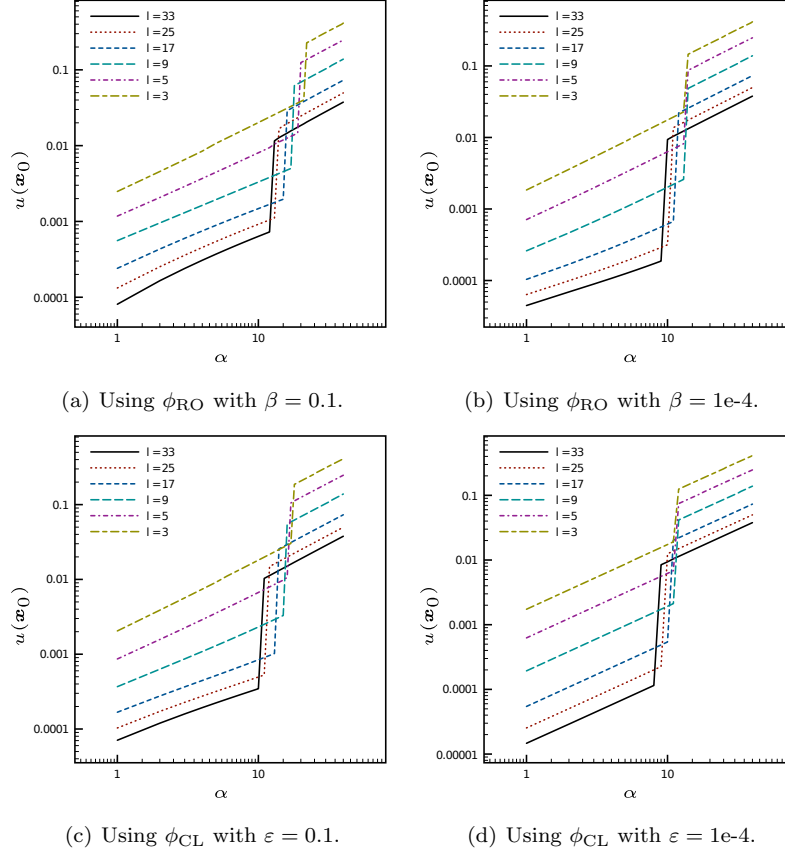
FIGURE 1. Fading test: value of $u(\boldsymbol{x}_0)$ for different length scales l
for the model based on (5) (top) and (6) (bottom).

translates, for given $u_n \in \mathbb{P}_0(\mathcal{S})$, into a sparse matrix $\boldsymbol{J}(\llbracket u_n \rrbracket)$ with a similar structure as appearing in finite difference discretizations with local stencils. In summary, the iteration (15) can be written in terms of the following $mn \times mn$-linear system:

$$\left(\boldsymbol{I} + \frac{\alpha}{2h} \boldsymbol{J}(\llbracket u_n \rrbracket) \right) \boldsymbol{U} = \boldsymbol{f}.$$

Here, $\boldsymbol{f}$ and $\boldsymbol{U}$ are suitably reshaped vectors representing the color values of the image f and the solution u_{n+1}, respectively. In order to solve this linear system efficiently, a preconditioned conjugate gradient method is applied. The stopping criterion of the iterative loop (15) is based on the increment

$$\frac{\|u_n - u_{n-1}\|_{L^\infty(\mathcal{S})}}{\|f\|_{L^\infty(\mathcal{S})}}.$$

4.2. Examples. In the following, the proposed algorithm is applied to three different examples.

4.2.1. Example 1: We first study the role of α as well as of the regularization parameters β and ε in the denoising model based on (5) and (6), respectively. In particular, we investigate how these quantities are related to fading. For this purpose, we apply the proposed DG algorithm to a white image of 101×101 pixels,

(a) Original image.   (b) Noisy image.   (c) Restored image.

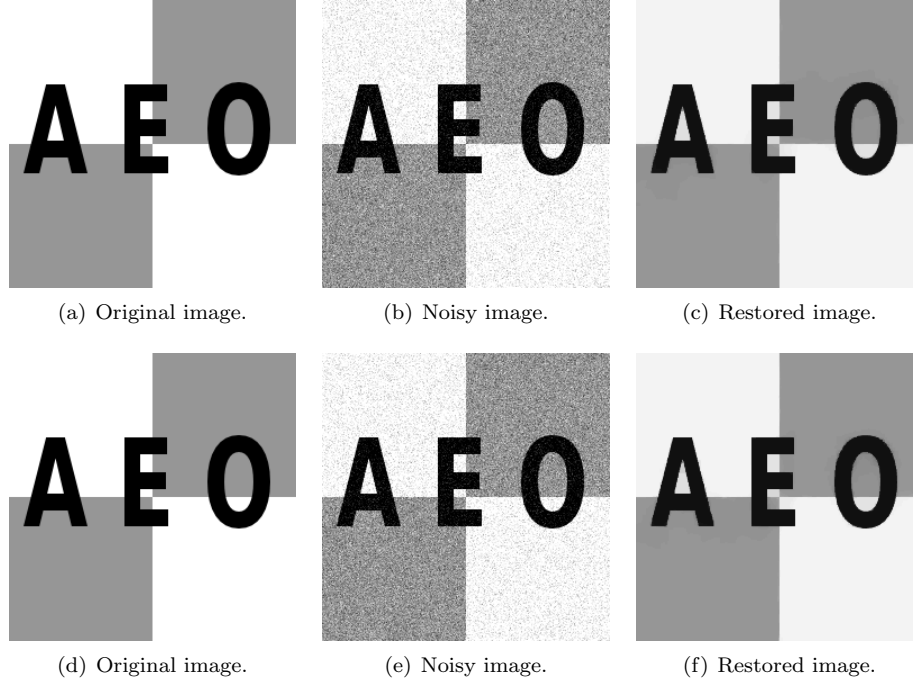(d) Original image.   (e) Noisy image.   (f) Restored image.

FIGURE 2. Original image (left), noisy image with white noise based on 10% standard variation (center), and the restored images (right) using ϕ_{RO} from (5) (top) and ϕ_{CL} from (6) (bottom) with $\beta = $ 1e-4 resp. $\varepsilon = $ 1e-4, and $\alpha = 30$.

with a black square of $l \times l$ pixels at its center $\boldsymbol{x}_0$, and ask the question of how the black color around the center of the image is fading out as α is increased. Considering a grayscale range of $[0, 1]$ (where 0 corresponds to 'black' and 1 corresponds to 'white'), we monitor the value $u(\boldsymbol{x}_0)$ of the restored image at the center with respect to different values of α and different lengths l, for both of the above denoising models, with different regularization parameters. The results are illustrated in Figure 1. They lead to the following observations:

- As α increases the fading increases also; indeed, since the jump term in the energy functional (7) controls the smoothing process in the image, this is perfectly sensible;
- There is a jump in the value of $u(\boldsymbol{x}_0)$ of approximately one order of magnitude at around $\alpha = 10$ that only depends moderately on the model and the regularization parameters used;
- As l increases the fading decreases.

Consequently, for a given noisy image, an appropriate value of α that limits fading of pixel blocks of length l up to a given tolerance, can be determined using the above tables. In particular, we remark that an appropriate choice of α is related to a characteristic size of objects in the image to be restored.

4.2.2. Example 2: The next example focuses on edge detection. Let us consider the image as illustrated in Figure 2(a) consisting of 256×256 pixels. The regularization parameters are set to $\beta = $ 1e-4 and $\varepsilon = $ 1e-4 for the denoising models

(a) Original image.   (b) Noisy image.   (c) Restored image.

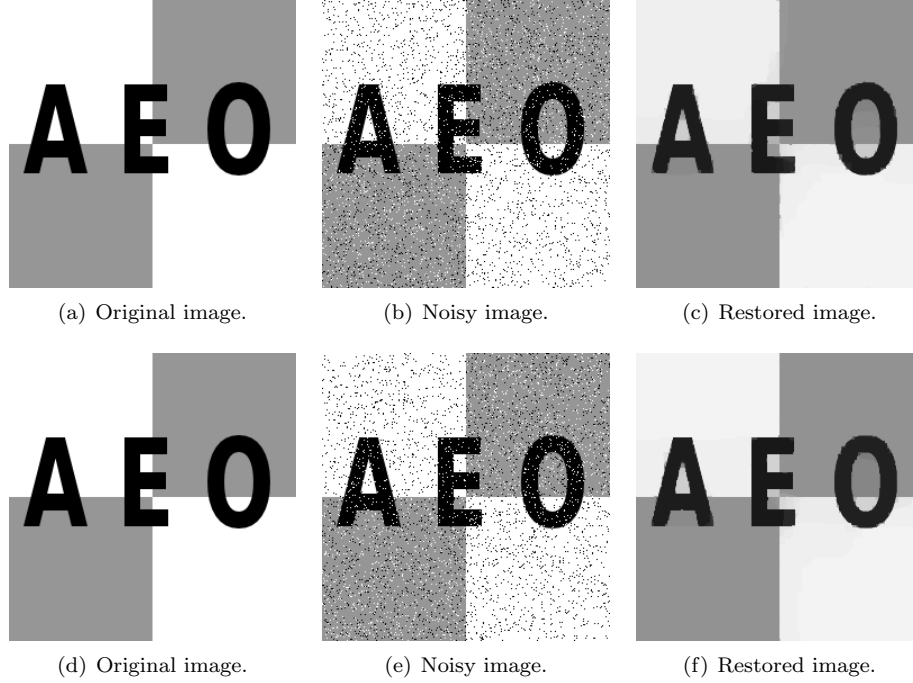(d) Original image.   (e) Noisy image.   (f) Restored image.

FIGURE 3. Original image (left), noisy image based on 10% salt and pepper noise (center), and the restored images (right) using ϕ_{RO} from (5) (top) and ϕ_{CL} from (6) (bottom) with $\beta = $ 1e-4 resp. $\varepsilon = $ 1e-4, and $\alpha = 60$.

based on (5) and (6), respectively. The tolerance for the stopping criterion of the increment is set to 0.01. We add either white (Gaussian) or salt and pepper noise in order to test the proposed algorithm.

In Figure 2, in addition to the original image, we present the noisy image with white noise based on 10% standard variation and the denoised images using ϕ_{RO} (Figure 2(c)) and ϕ_{CL} (Figure 2(f)), with $\alpha = 30$. The algorithm (15) required 9 respectively 8 iterations to converge within the prescribed increment tolerance.

In Figure 3, we present the original image, the noisy image with salt and pepper noise of 10%, as well as the denoised image using ϕ_{RO} (Figure 3(c)) and ϕ_{CL} (Figure 3(f)), with $\alpha = 60$. Here, the sequence of images generated by (15) converged after 36 respectively 41 iterations.

4.2.3. Example 3: Finally, we apply the proposed scheme to an MRI image[1] as illustrated in Figure 4(a). The images consists of 640×588 pixels. We add white noise of 10% standard variation and perform the denoising computations for different values of $\alpha = 5, 7.5, 10$. The restored images, using ϕ_{CL} from (6), with regularization parameter $\varepsilon = $ 1e-4, are illustrated in Figures 4(c), 4(f) and 4(i). The tolerance for the stopping criterion of the increment is set to 0.01 which required 8, 10 respectively 10 iterations to converge.

---

[1]http://en.wikipedia.org/wiki/File:Mrt_big.jpg

(a) Original image.   (b) Noisy image.   (c) Restored image.

(d) Original image.   (e) Noisy image.   (f) Restored image.

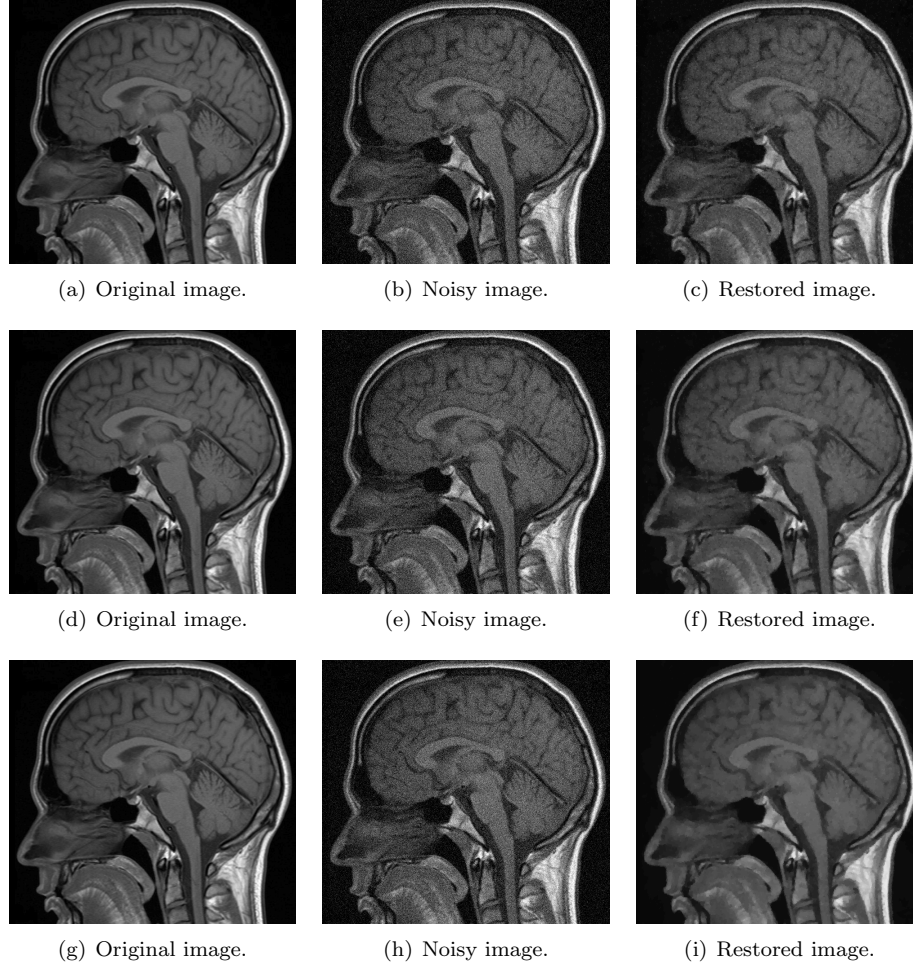(g) Original image.   (h) Noisy image.   (i) Restored image.

FIGURE 4. Original image (left), noisy image based on white noise with 10% standard variation (center) and the restored images (right) for three different values of $\alpha = 5, 7.5, 10$ (from top to bottom), using ϕ_{CL} from (6) with $\varepsilon = 1\mathrm{e}\text{-}4$.

5. Conclusions

In this paper, we have introduced a zero-order discontinuous Galerkin method for image denoising based on a discrete total variation approach. The proposed scheme is obtained by minimizing a suitable discrete energy functional. The smoothing of noisy images is taken care of by means of a discrete gradient which is expressed in terms of a jump operator. We note, however, that alternative possibilities, including lifting operators (see, e.g., [1]) could be applied within the given DG framework. In this way, our approach can be seen as a generalization of standard finite difference stencils or finite volume schemes as applied in, e.g., [14]. Remarking the fact that the DG scheme in this paper has a highly parallelizable character, future work will be dedicated to the development of an efficient implementation of the proposed method on graphical processing units (GPU).

References

[1] D. N. Arnold, F. Brezzi, B. Cockburn, and L. D. Marini. Unified analysis of discontinuous Galerkin methods for elliptic problems. *SIAM J. Numer. Anal.*, 39:1749–1779, 2001.

[2] G. Aubert and L. Vese. A variational approach in image recovery. *SIAM J. Numer. Anal.*, 34(5):1948–1979, 1997.

[3] A. Buades, B. Coll, and J. M. Morel. A review of image denoising algorithms, with a new one. *Multiscale Model. Simul.*, 4(2):490–530, 2005.

[4] A. Chambolle, S. E. Levine, and B. J. Lucier. An upwind finite-difference method for total variation–based image smoothing. *SIAM J. Imag. Sci.*, 4:277–299, 2011.

[5] A. Chambolle and P. L. Lions. Image recovery via total variation minimization and related problems. *Numer. Math.*, 76:167–188, 1995.

[6] J. Darbon and M. Sigelle. Image restoration with discrete constrained total variation, Parts I + II. *J. Math. Imaging and Vision*, 26, 2006.

[7] W. B. Liu and J. W. Barrett. Quasi-norm error bounds for the finite element approximation of some degenerate quasilinear elliptic equations and variational inequalities. *RAIRO Modél. Math. Anal. Numér.*, 28(6):725–744, 1994.

[8] J. Nečas. *Introduction to the Theory of Nonlinear Elliptic Equations*. John Wiley and Sons, 1986.

[9] S. Osher, M. Burger, D. Goldfarb, J. Xu, and W. Yin. An iterative regularization method for total variation-based image restoration. *Multiscale Model. Simul.*, 4:460–489, 2005.

[10] S. Osher, A. Solé, and L. Vese. Image decomposition and restoration using total variation minimization and the h^{-1} norm. *Multiscale Model. Simul.*, 1:349–370, 2003.

[11] L. Rudin and S. Osher. Total variation based image restoration with free local constraints. In *Proceedings of the IEEE International Conference on Image Processing*, volume 1, pages 31–35, Austin, TX, 1994.

[12] L. Rudin, S. Osher, and E. Fatemi. Nonlinear total variation based noise removal algorithms. *Phys. D*, 60:259–268, 1992.

[13] S. Teboul, L. Blanc-Feraud, G. Aubert, and M. Barlaud. Variational approach for edge-preserving regularization using coupled PDE's. *IEEE Trans. Image Proc.*, 7(3):387–397, 1998.

[14] M. von Oehsen. *Multiscale Methods for Variational Image Denoising*. PhD thesis, Medizinische Universität Lübeck, 2002.

[15] E. Zeidler. *Applied functional analysis*, volume 108 of *Applied Mathematical Sciences*. Springer-Verlag, New York, 1995. Applications to mathematical physics.

LJLL UPMC, 75252 Paris Cedex 05, France
E-mail: `stamm@ann.jussieu.fr`

Mathematics Institute, University of Bern, Sidlerstrasse 5, CH-3012 Switzerland
E-mail: `wihler@math.unibe.ch`